A mathematical model for spin coating of polymer resists

Warren W. Flack, David S. Soong, Alexis T. Bell, and Dennis W. Hess
Department of Chemical Engineering, University of California, Berkeley, California 94720

(Received 29 September 1983; accepted for publication 10 November 1983)

The success of lithographic processes in microelectronics fabrication depends on the reproducible generation of desired polymer resist film thickness and profile uniformity. Numerous process variables affect the outcome of spin coating of resists on wafers. A thorough understanding of the intricate interdependence of process parameters is essential to guide future process design and improvement. A mathematical model is derived to elucidate the dominant mechanisms governing film formation. The non-Newtonian character of the resist solution is taken into account, as well as the changes in resist viscosity and solvent diffusivity with changing polymer concentration. Results obtained from this model show that polymer film thickness is controlled by convective radial flow of the resist solution and solvent evaporation. The former process governs film thickness during the early stages of the process, while the latter becomes significant in later stages. The model accurately describes the experimentally observed dependence of film thickness on the variables affecting the spin-coating process.

INTRODUCTION

Spin coating of resist films on silicon wafers is an important step in the fabrication of integrated circuits, Film formation is accomplished by dispensing a fixed amount of polymer solution onto a wafer. The wafer is thin rotationally accelerated up to a preset speed. The resist solution flows radially outward due to centrifugal force, reducing the fluid layer thickness, Evaporation of solvent from the resist solution continuously changes the fluid composition and thereby the rheological properties of the fluid. Understanding the film formation process is critical to determining the outcome of the entire lithographic process. This has become particularly so in recent years as device features shrink to submicron sizes. Resist film uniformity must be held within a small tolerance to minimize exposure artifacts, Currently, achievement of this requirement demands a significant amount of time and effort to characterize a new resist material so that a viable spin-coating process can be established. Appreciable simplification of this process could be attained if a quantitative model were available to describe the fluid behavior during spin coating.

A number of theoretical as well as experimental studies of the spin-coating process have been presented in the literature. [1-11] Empirical correlations have been generated based on a large number of experiments with different process parameters. [4,7,9-11] It has been established that the initial volume of the fluid dispensed on to the rotating disk and the rate of fluid delivery (i.e., dispense speed during a brief period of slow rotation preceding spinning to spread out the fluid) have a negligible effect on the final film thickness. On the other hand, the final film thickness is a strong function of the resist viscosity and final spin speed. An increase in angular velocity decreases the film thickness. An inverse power-law relationship generally holds for the thickness dependence on the final spin speed. For a given speed, the film thickness decreases rapidly at first, but then slows down considerably at longer times. [1] Increasing the polymer concentration in the resist results in thicker films, presumably because of the increased fluid viscosity.

Previous attempts to model the spin-coating process have been based on several major simplifying assumptions. Most treatments have assumed either Newtonian or power-law behavior with constant rheological properties during the process. [1-3,5,6,8] The neglect of solvent evaporation on the spin-coating process is a significant limitation of these efforts. During spinning. solvent evaporation drastically changes the rheological properties of the fluid, which in turn affects the rate at which the film thickness decreases with time. Only in the work of Meyerhofer[8] has an effort been made to account for the effects of solvent evaporation on resist viscosity and the spin-coating process. To facilitate the numerical computations, it was assumed that the process is composed of two limiting steps. At short times, the film thickness variation due to solvent evaporation was ignored. Beyond a certain critical point, it was assumed that fluid loss was due only to evaporation, and not to radial flow. The transition from one loss mechanism to the other was calculated to be the point at which the rates of the two loss processes become equal.

This paper describes a detailed numerical simulation of the spin-coating process. The model developed here takes into account changes in the resist properties resulting from solvent evaporation and the non-Newtonian character of the rheological behavior of the resist. The model is evaluated by comparing predicted film thickness and thickness profile with those observed experimentally for a variety of spin-coating conditions.

THEORY

The spin-coating process is described using the cylindrical coordinate system shown in Fig. 1. The system is characterized by disk radius R and angular velocity ω. Film thickness δ is a function of radial distance r. The value of δ changes with rime during spinning.

The major assumptions in this model are summarized below.

(1) Fluid flow is rotationally symmetrical. This assumption is consistent with experimental observation and re-

 0021-8979/84/161199-08$02.40

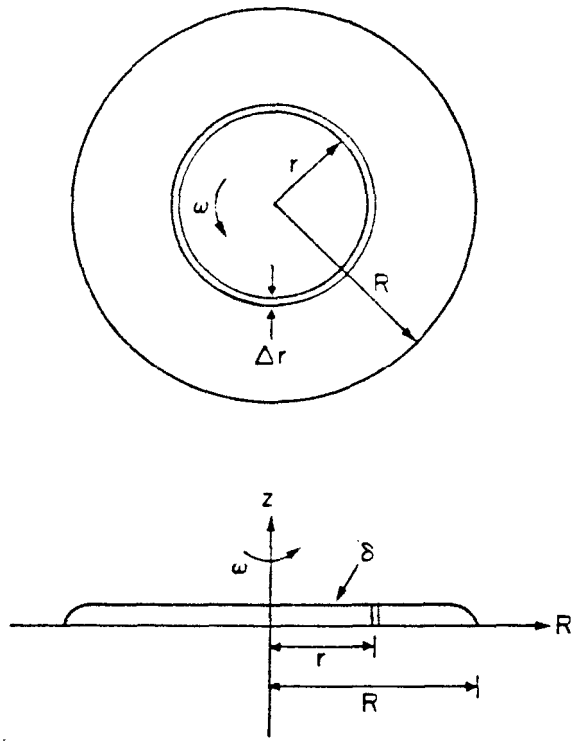

FIG. 1. Overhead and side views of the coordinate system used to describe resist spin coating. The wafer revolves along the z axis at an angular speed ω. The disk has a radius R. Film thickness δ is a function of time and radial positron r.

moves the need to consider angular dependence in the ensuing analysis.

(2) Fluid flow is restricted to the radial direction. This lubrication approximation greatly simplifies the equations of continuity and motion. This assumption is supported by the observation that δ is not a strong function of r.

(3) Surface tension forces are neglected. Introduction of this assumption only affects the validity of the model in the immediate vicinity of a thin ring surrounding the edge of the wafer.

(4) Density of the fluid stays constant. Since the polymer and solvent have similar densities, this assumption is realistic and leads to a significant simplification of the mathematics.

(5) The fluid temperature and the partial pressure of the solvent in the spinner chamber remain constant. A simple order-of-magnitude calculation confirms that evaporation of solvent from a thin film does not lead to a significant change in the film temperature.

The radial velocity v_r is governed by the continuity equation. Taking the lubrication approximation to be valid, we have

$$v_r = \psi(z)/r. \tag{1}$$

The radial velocity v_r is, thus, separable into a z-dependent function ψ and an explicit r dependence.

The equation of motion for the case of unsteady-state flow with the above velocity function is Riven by

$$\frac{\partial \psi(z)}{\partial t} = \frac{\psi^2(z)}{r^2} + r^2\omega^2(t) + \frac{\eta(c)}{\rho}\frac{\partial^2 \psi(z)}{\partial z^2} + \frac{\partial \eta(c)}{\partial z}\frac{1}{\rho}\frac{\partial \psi(z)}{\partial z}, \tag{2}$$

where η and ρ are the viscosity and density of the fluid, and $\omega(t)$ is the rotational speed of the wafer. The boundary and initial conditions are $\psi(t,0) = 0$ (no slip condition), $\partial\psi(t,\delta)/\partial z = 0$ (no momentum transfer at liquid-air interface), and $\psi(0,z) = 0$ (initially stationary disk).

The solvent concentration (either weight fraction or volume fraction) in the resist film is governed by the following mass balance:

$$\frac{\partial c}{\partial t} + \frac{\psi(z)}{r}\frac{\partial c}{\partial r} = D(c)\frac{\partial^2 c}{\partial z^2} + \frac{\partial D(c)}{\partial z}\frac{\partial c}{\partial z}. \tag{3}$$

The boundary and initial conditions for Eq. 3 are $c(t,\delta) = c_0$ (fixed concentration at liquid-air interface), $\partial c(t,0)/\partial z = 0$ (no mass transfer at solid-liquid interface), and $c(0,z) = c_b$ (initial bulk concentration), where c_0 is the concentration of solvent in equilibrium with the vapor partial pressure in the chamber, and c_b is that in the bulk fluid initially dispensed onto the disk. The second term on the left-hand side of Eq. (3) can be neglected completely, as its magnitude is small compared with the other terms.

The time-dependent variation in the thickness of each differential slice of the resist film is described by the following equation.

$$\left.\frac{\partial \Delta z}{\partial t}\right|_z = \frac{2\left(\int_z^{z+\Delta z} \psi|_{r-\Delta r}\,dz - \int_z^{z+\Delta z} \psi|_r\,dz\right)}{(2r\Delta r - \Delta r^2)} + \frac{D}{\rho}\left(\left.\frac{\partial c}{\partial z}\right|_{z+\Delta z} - \left.\frac{\partial c}{\partial z}\right|_z\right). \tag{4}$$

The first term on the right-hand side represents material loss due to the convection, whereas the second term accounts for solvent diffusion. Note that unless the radius is much greater than the radial step Δr, the second order effect must be accounted for in the denominator of the first term on the right-hand side. Previous models [1,2,5,6,8] have always used the linear form, resulting in an infinite singularity at the center of the disk. The partial differential of δ with respect to time, $\partial\delta/\partial t$, is obtained at each value of r by summing the contributions from Eq. (4) from $z = 0$ to $z = \delta$.

The dependence of the solvent diffusivity on solvent concentration in the resis film is described by

$$D = D_0(T)Q(c,T), \tag{5}$$

where D_0 is the temperature-dependent front factor, and Q is the concentration-dependent free-volume factor. The form of Q is given by the Fujita–Doolittle equation.[12,13]

$$Q(c,T) = \exp\left(\frac{c}{A + Bc}\right), \tag{6}$$

where A and B are temperature-dependent parameters.

Viscosity of the system as a function of concentration is affected by both free-volume change and entanglement formation as the solvent evaporates.[14] The former can be accommodated in a manner similar to the concentration-dependent diffusivity, whereas proper consideration of the latter must invoke scaling concepts[15] to account for chain-chain interactions. For the present effort, we assumed the viscosity function to be a product of two components as shown below:

$$\eta = (\eta_0/Q)(1 - c)^x, \tag{7}$$

where Q in the denominator is the same free-volume factor as in Eq. (6), and the power-law dependence on polymer concentrations $(1 - c)^x$ conforms to scaling concepts. If the free-volume term $(1/Q)$ were not included, the exponent x itself would become a function of concentration and temperature. However, separation of the viscosity dependence into free-volume and entanglement terms allows a fixed number $x = 2.33$ to be used over wide temperature and concentration ranges.[16]

The form of the viscosity relation given above does not yet take into account the non-Newtonian feature of the resist solution. When the rotational speed is high, the fluid is sheared to a large extent, inducing appreciable shear thinning of the material. Hence, approximation of the fluid behavior by a Newtonian constitutive equation leads to inaccurate predictions The Newtonian model not only predicts too thick a film, but also gives too weak an angular speed dependence of the film thickness, as will be shown below.

To accommodate non-Newtonian effects, a realistic constitutive equation is used for the shear-rate dependent viscosity.[17-19] The overall system viscosity is divided into contributions from the polymer and remaining solvent:

$$\eta = \eta_p + \eta_s = \frac{\eta_{p0}}{1 + b\,\mathrm{II}^{a/2}} + \eta_s , \qquad (8)$$

where η is the total system viscosity, η_p and η_s are the polymer and solvent contributions, b and a are parameters characterizing the onset of non-Newtonian behavior and the slope of the power-law relationship for the shear-rate dependence. The quantity η_{p0} is the polymer contribution to the viscosity at zero shear and is taken to be described by Eq. (7). II is a measure of the local flow intensity related to the second invariant of the strain rate tensor. For the cylindrical coordinate system under consideration,

$$\mathrm{II} = 4\left[\left(\frac{\psi}{r^2}\right)^2 + \frac{1}{r}\left(\frac{\partial \psi}{\partial z}\right)^2\right]. \qquad (9)$$

Note that in this approach, the shear-thinning behavior is attributed to the polymer component of the solution only and is taken into account in the constitutive equation by the first term of the right-hand side of Eq. (8).

The non-Newtonian parameters a and b in Eq. (8) are functions of concentration. Liu, Soong. and Williams[19] examined a large number of data sets for different polymer-solvent pairs at various temperatures, and found that values for a at different concentrations follow a consistent trend, which is described by the relationship $a = k_1 \log(1 - c) + k_2$ where k_1 and k_2 are universal constants.[19] In addition, b was found to conform to the relationship $b = k_0 \eta_{p0}^a$.

The conservation and constitutive equations form a complete description of the spin-coating process. These equations are ,however, coupled and highly nonlinear, making exact numerical solution difficult and time-consuming. To expedite the determination of v_r, c, and δ as functions of time and spatial position. the procedure outlined below was adopted.

The approach begins by recognizing that the dependence of c on z and t can be determined independent of knowing $\Psi(z)$, since the second term on the left-hand side of Eq. (3) is small. The function $c(z,t)$ can then be used to determine the solvent concentration dependence of η, which is required in order to proceed with the solution of Eq. (2) for $\psi(z,t)$. Finally the rate of change in the film thickness is determined by introducing $\Psi(z,t)$ and $c(z,t)$ into Eq. (4) and summing from $z = 0$ to $z = \delta$.

During the initial stages of the spin-coating process, Eq. (3) can be solved analytically by use of a similarity transformation. To do so, we define the variable $y = z/t^{1/2}$ The solution of Eq. (3) in terms of the transformed variable gives

$$c = c_0 + (c_b - c_0)\left[\int_0^y \frac{1}{D}\exp - \left(\frac{1}{2}\int_0^{y'} \frac{y'}{D}\,dy'\right) dy'' \Big/ \int_0^{\delta} \frac{1}{D}\exp - \left(\frac{1}{2}\int_0^{y'} \frac{y'}{D}\,dy'\right) dy''\right], \qquad (10)$$

where $D = D(y)$ Equation (10) is, strictly speaking, only valid if the liquid layer is semi-infinite. In practice, it was found that within a few tenths of a second, the solvent concentration very near the gas-liquid interface decreased to a level ($c_0 = 0.1$ for our experimental condition), which significantly decreased the solvent diffusivity. Formation of this diffusion barrier greatly impedes the further loss of solvent by evaporation, until the last stages of the spin-coating process. At that point. the residual film becomes very thin (~1 μm) and the solvent profile can now penetrate back to the liquid-solid interface. When this happens, c_b begins to decrease with time. The decrease in c_b can be described by Eq. (11).

$$c_b(t + \Delta t) = c_b(t) + \frac{D}{\delta}\Delta t \left.\frac{\partial c}{\partial z}\right|_{z=0} . \qquad (11)$$

Equation (2) for $\Psi(z,t)$ is solved numerically using a finite difference approach. To do so, the partial differential equation is approximated by the following ordinary differential equation

$$\frac{\Delta \psi}{\Delta t} = \frac{\psi^2}{r^2} + r^2\omega^2 + \frac{\eta}{\rho}\frac{d^2\psi}{dz^2} + \frac{1}{\rho}\frac{d\eta}{dz}\frac{d\psi}{dz} . \qquad (12)$$

In Eq. (12), $\Delta\Psi$ is the difference in the values of Ψ at $t + \Delta t$ and t. It is assumed that for each value of r, the change in Ψ over Δt is small, so that η and $d\eta/dz$ can be calculated from $\Psi(z,t)$ and $c(z,t)$. The function $\Psi(z,t + \Delta t)$ is then obtained by solving Eq. (12) by a modified fourth-order Runge-Kutta technique. The solution is initiated at the liquid-solid interface where $\Psi = 0$ at all times. A guess is then made for $d\Psi/dz$ at this interface, and the solution for $\Psi(z,t + \Delta t)$ is generated. The value of $d\Psi/dz$ at $z = \delta$ is now calculated and compared with the boundary condition of $d\psi/dz|_{z=\delta} = 0$. If the agreement is poor, a new estimate of $d\psi/dz|_{z=0}$ is obtained, and a new solution for Ψ is generated. Iteration is continued to the point of convergence on the boundary condition at $z = \delta$. At the end of calculation, the final film thickness is adjusted by decreasing it by 10% for comparison with experimental data. This step is warranted because experimentally it was found that post-spin baking of the resist film drives off the residual solvent and reduces the thickness by 10%.

The procedures described above were used at each value of r to generate the corresponding representations for $c(z,t)$, $\Psi(z,t)$, and $\delta(t)$. The algorithm used for the solutions of Eqs. (2), (3), and (4) were written in PASCAL and were executed on a Compupro S- 100 Bus Microcomputer with 8086 Mi-

croprocessor and 8087 Math Coprocessor. The CPU time required for one execution of the program was 12 h.

EXPERIMENT

The resist system chosen for experimental study was a standard electron beam resist, poly(methyl methacrylate) (PMMA). Resist solutions of 4, 6, and 9% PMMA in chloro - benzene were purchased from KTI Chemicals. A 2% solution was prepared by dilution. Previous work by Wu *et al.*[20] has shown that this polymer has a number average molecular weight M_n of approximately 1.25×10^5 and a polydispersity index M_w/M_n of 3.0.

The substrates used were unoxidized 2- and 3-in.-diam silicon wafers. The wafers were cleaned using the following standard procedure: (1) a 10-min acetone soak in an ultrasonic bath: (2) a 1-min rinse in deionized (> 16 mΩ cm) water; (3) a 15-min soak at 60 °C in freshly mixed 5:1 18-M sulfuric acid to 30% hydrogen peroxide; (4) a repeated 1-min rinse in deionized (DI) water; (5) a 20-set dip in 10:1 water to 49% hydrofluoric acid: (6) a final 1-min rinse in DI water. The cleaned wafers were stored in deionized water until resist coating was to be performed.

A Headway Research spinner was modified to permit selection and control of the rate at which the final rotational speed is approached. Unless otherwise specified, a 1-sec ramp was used for most runs. The vacuum chuck and spinner bowl were enclosed in a glove box, which was vented by a vacuum line.

The freshly cleaned wafers were transferred from the DI water to the spinner glove box. Each wafer was then centered on the chuck and spun at final speeds from 500 to 4000 rpm for 1–2 min until dry. Approximately 2 ml of resist solution was then dispensed onto the wafer. The spinner was restarted and spun until the resist film was dry. Drying times vaned from 20 sec to over 2 min, depending on the polymer concentration of the resist solution. High quality, reproducible films were obtained in this manner.

After spinning, the wafers were baked in a convection oven at 160 °C for 1 h, to remove the residual solvent. This drying process reduced the film thickness by approximately 10%. Film thickness profiles were measured with an IBM 7840 Film Thickness Analyzer. This instrument uses an interferometric technique to determine the film thickness. For the purpose of these calculations, the refractive index of the film was taken to be 1.49.[20]

The viscosities of dilute PMMA solutions were determined using an Ubbelohde glass capillary kinematic viscometer. A calibration curve was established for the viscometer using glycerol-water solutions of known viscosity.[21] The viscosities of 2, 4, and 6% PMMA in chlorobenzene were then determined. The viscosity of a 9% solution was determined using a falling sphere viscometer. The Reynolds number for this measurement was kept below 0.1 to ensure laminar flow.

Concentrated solutions of PMMA were studied using a CSI CS-203 Melt Elasticity Tester.[22] A polymer sample was placed in the annular space between an outer cup and a center rod. The sample was then sheared by steadily rotating the Outer cup while the center rod was restrained from rotation by a lever arm acting against a force transducer. The shear-rate-dependent viscosities of 40% and 60% PMMA in chlorobenzene were determined using this instrument. These provided information concerning the non-Newtonian properties of the resist solutions.

RESULTS AND DISCUSSION

Determination of constitutive parameters

The theoretical model described in this paper requires the identification of five parameters, D_0, A, B, η_0 and k_0. With the exception of D_0 the value of each parameter was determined by fitting experimental data to the appropriate constitutive equation, Figure 2 shows low-shear-rate viscosity data for several solutions. Numerical values for the model parameters are given in Table I. The solid curve is the best fit to these data by Eq. (7). Figure 3 presents rate-dependent viscosity data for the more concentrated solutions meaured with the metal elasticity tester, The slopes of the power-law region for the two solutions fall in the range previously reported for other systems.[19] Once a is determined this way, k_0, characterizing the onset of non-Newtonian behavior, can be obtained by a nonlinear fit of the data with Eq. (8)(see Table I). The solid curves in Fig. 3 are then drawn using this fitted value of k_0 and Eq. (8).

Since the diffusivity equation [Eq. (5)] follows the functional form of the Fujita–Doolittle equation, the only remaining constitutive parameter is the diffusion preexponential coefficient D_0. Lütje and Meyerhoff[23] have measured the

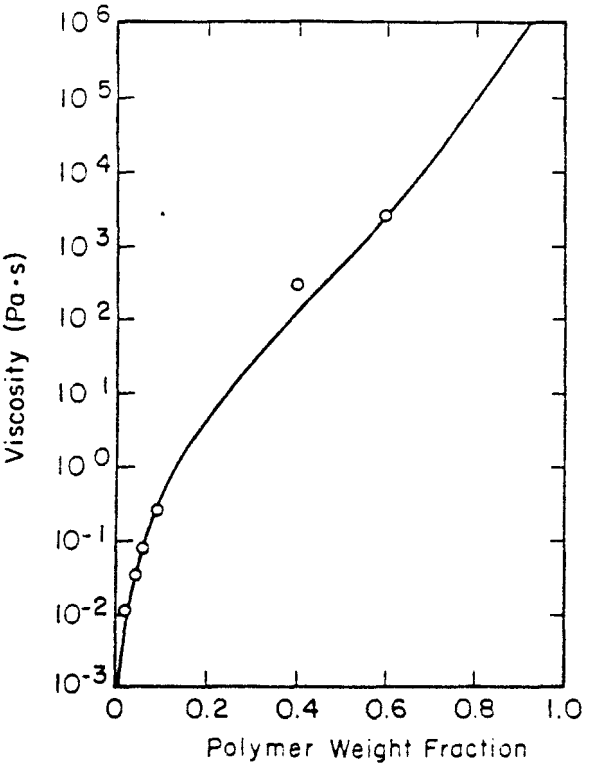

FIG. 2. Experimental viscosity data (circles) and model predictions (solid curve) based on the constitutive relationship embodying free-volume and coil-coil interaction considerations. The model provides a quantitative description of the concentration dependence of the viscosity.

TABLE I. Constitutive equations and numerical values for the model parameters.

Viscosity

$$\eta(c, \mathrm{II}) = \frac{\eta_{p0}(c)}{1 + b\,\mathrm{II}^a} + \eta_s$$

$$\eta_{p0}(c) = \eta_0 / \exp\left(\frac{c}{0.043 + 0.040c}\right) \times (1 - c)^{2.33}$$

$$\eta_0 = 7.06 \times 10^7 \text{ (poise)}$$

$$\eta_s = 0.008 \text{ (poise)}$$

$$\mathrm{II} = 4\left[\left(\frac{\psi}{r^2}\right)^2 + \frac{1}{r}\left(\frac{\partial \psi}{\partial z}\right)^2\right]$$

$$a = 0.074 \log(1 - c) + 0.904$$

$$b = 0.1\,\eta_{p0}^a$$

Diffusivity

$$D(c) = D_0 \exp\left(\frac{c}{0.043 + 0.040c}\right)$$

$$D_0 = 7.78 \times 10^{-12} \text{ (cm}^2\text{/s)}$$

diffusivity of a 4% solution of PMMA in toluene to be 9x 10^{-11} m^2/s. We assume the diffusivity of the chlorobenzene solution to be comparable to that of the toluene solution, as the solvent molecules are similar in size and shape. The value of D_0 can be determined by requiring agreement between the measured diffusivity and Eq. (5). The value of D_0 thus obtained is given in Table I.

Comparison of model predictions with experimental results

Experimental results and model predictions based on the non-Newtonian analysis are summarized on a log-log plot of average film thickness as a function of the final spin speed (Fig. 4). Excellent agreement is seen between the model predictions and experimental data for 9, 6, and 4% resist solutions. Serious discrepancy occurs for the 2% polymer solution, the calculated thicknesses being significantly thicker than the experimental values. (However, the slope of the predicted curve is in agreement with the data.)The most likely source of this error is neglect of surface forces in the model. A 2% polymer solution spun at 1000 rpm leaves a final film that is approximately 200 nm thick. A KTI PMMA molecule has a typical dimension on the order of 50 nm.[24] The final film thus corresponds to only a few monolayers of polymer. The failure to model the spin coating of films from a 2% solution is not a serious problem since solutions with a polymer weight fraction below about 4% are generally not used in commercial practice. The reason for this is that very thin films often contain a large number of pinholes.

The significance of taking into account the non-Newtonian characteristics of the resist solution is illustrated in Fig, 5. It is apparent that the assumption of Newtonian behavior leads to a weaker dependence of film thickness on spin speed than is observed experimentally, and one which is indepen-

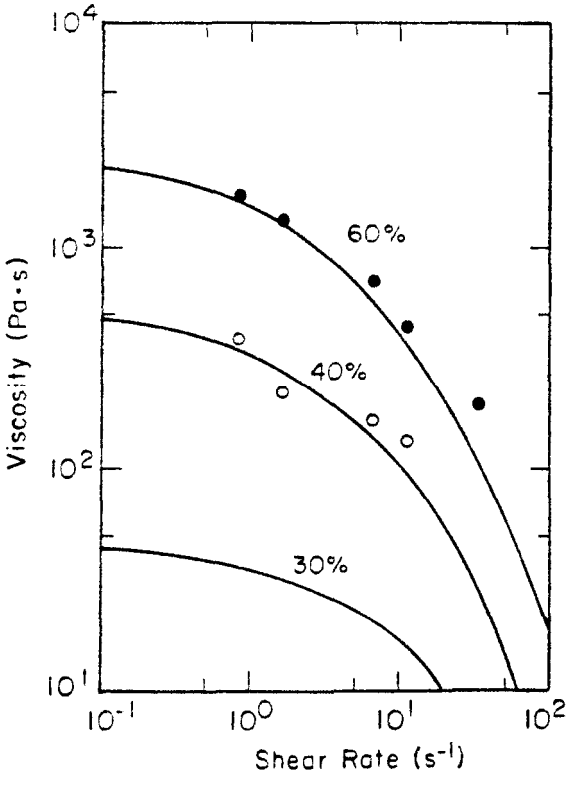

FIG. 3. Viscosity data measured with the melt elasticity tester and computed curves based on the non-Newtonian constitutive relationship The only adjustable model parameter characterizing shear-thinning behavior k_0 is estimated by fitting the two sets of data shown here. Once this parameter is known. viscosity master curves at any other concentrations, e.g., 30%, can be easily calculated.

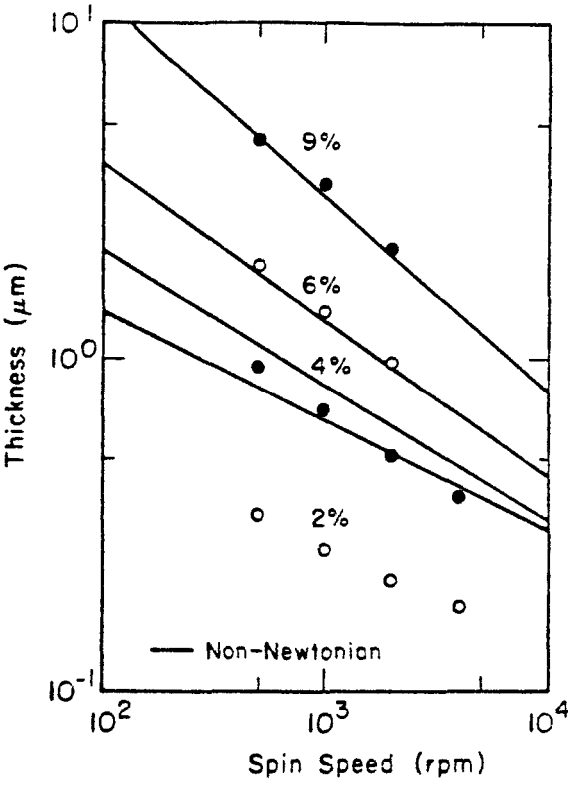

FIG 4. Comparison of measured and predicted average film thickness as a function of final spin speed for several resist concentrations. Increasing speed decreases film thickness, whereas increasing initial solution concentration leads to thicker deposits. Model predictions agree well with expenmenial observations for reasonably concentrated solutions At low initial concentrations, e.g., 2% to 4%. the model overpredicts the final film thickness.

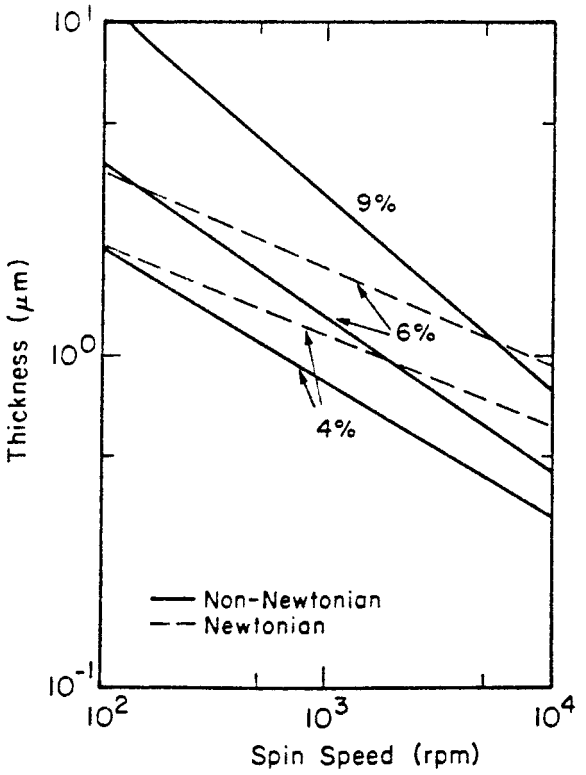

FIG. 5. Calculated film thickness as a function of spin speed and concentration. Solid curves represent the non-Newtonian analysis, while dotted curves are for the Newtonian model. Neglect of shear-thinning behavior not only results in overprediction of film thickness but also underprediction of its dependence of spin speed.

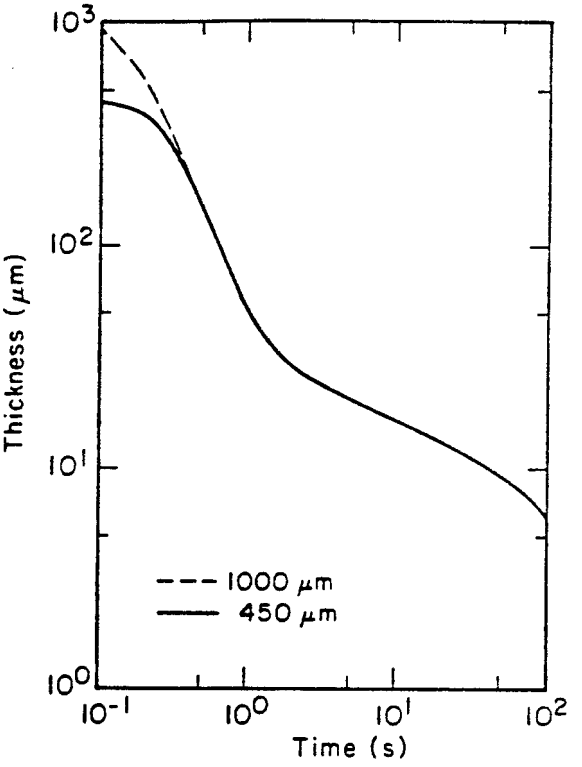

FIG. 6. Effect of initial fluid volume on the average film thickness as a function of time during spinning. The film thickness drops rapidly at first, essentially eliminating the differences between the two cases by the end of the first second into the process.

dent of polymer concentration in the initial resist. The non-Newtonian model not only gives quantitative predictions of the film thickness. but also generates the correct dependence on spinner speed. The dependence on spinner speed is stronger for the higher concentration solutions. This is attributable to the more prominant non-Newtonian behavior of the resist at higher concentrations.

Model predictions for prespin film thicknesses of 450 and 1000 μm (6% solution) are shown in a log-log plot of average thickness as a function of time (Fig. 6). The choices of 450 and 1000 μm film thickness correspond to uniform flooding of a 3 in water with 2 and 4.5 ml of resist solution, respectively. The initial thickness difference between the 1000 and the 450-μm film diminishes rapidly as the wafer is accelerated. After approximately 1 s, the thickness versus time profiles become independent of the initial volume of resist dispensed. This result is in complete agreement with the experimental observations of Daughton, O'Hagen, and Givens.[9]

The contributions of radial convection and evaporation to the thinning of the resist film were examined for the case of 450-μm prespin thickness (6% solution), spun at a final spin speed of 1000 rpm. The average film thickness history of this case was shown in Fig. 6. Figure 7 gives the thickness loss rates attributed to convective flow and solvent evaporation as functions of time. Convection clearly dominates during the early stages of the process, but evaporation becomes the dominant loss process at longer times. The convective loss curve exhibits a sharp rise initially. This is due to spinner

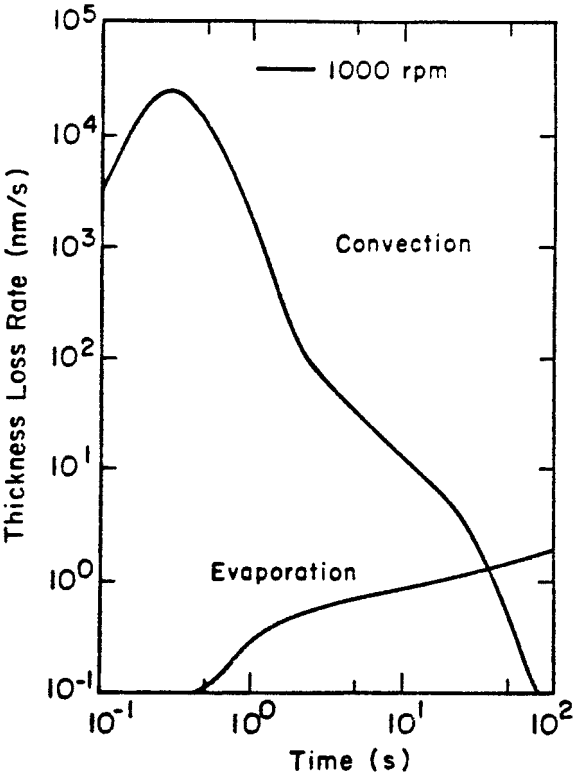

FIG 7. Calculated thickness loss attributed to convective motion and solvent evaporation for processes involving a 6% KTI PMMA solution spun at 1000 rpm Convection governs early phases, whereas evaporation contnbutes primarily to thickness reduction in later stages The initial rise in convective loss is caused by spinner acceleration.

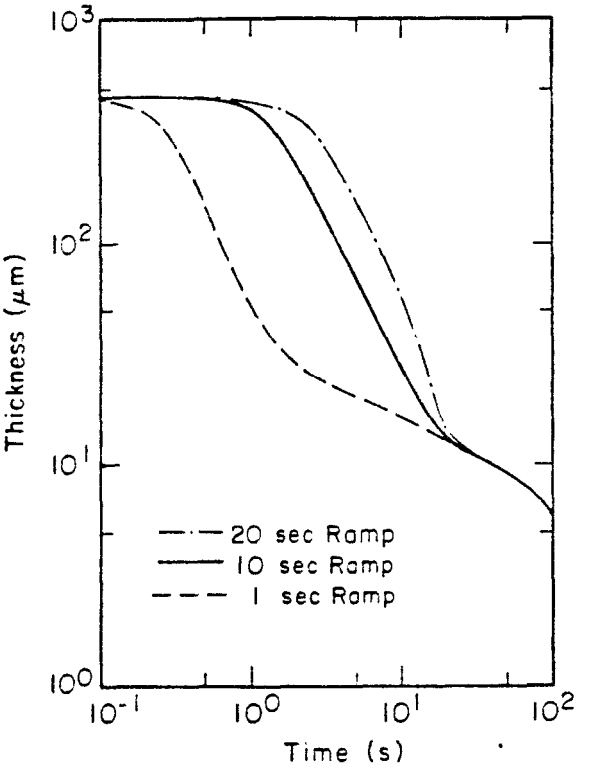

FIG 8. Effect of spinner acceleration rate on film thickness variation The spinner is linearly accelerated to 1000 rpm within the designated number of seconds.

acceleration, which increases the effectiveness of the spinner to throw off fluid radially The rapid decrease in the rate of convective loss following the maximum is due to the combined effects of the increasing viscosity of the resist solution and the increasing effects of the no-slip boundary condition at the wafer surface. The rise in the rate of evaporative loss is due totally to the decrease in film thickness. This is moderated, of course, by the rapidly decreasing solvent diffusivity.

The gradual trade-off between the two loss mechanisms seen in Fig. 7 conceals the complex interplay of various process variables. The loss mechanisms are closely coupled, and the relationships among the process variables can be subtle. Hence, the net effects of a change in one process variable cannot be projected intuitively. For example, increasing solvent partial pressure in the chamber would be expected to reduce solvent evaporation and hence contribute to forming a thicker film. However, the slower drying process also retards the increase in the fluid viscosity and thereby enhances convective loss. This latter process contributes to forming a thinner film. It is therefore apparent that in order to understand how solvent vapor pressure, or for that matter any other variable, affects the final film thickness, it is necessary to utilize the complete model.

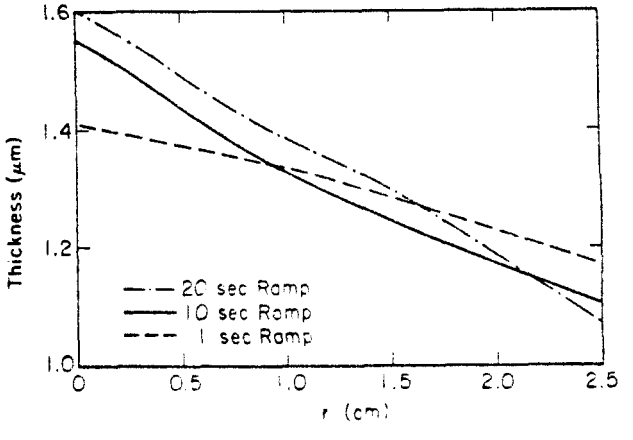

FIG 9. Calculated final thickness profiles for different ramp rates Increasing the rate of acceleration leads to a more uniform final film All curves exhibit gradual tapering towards the edge of the disk.

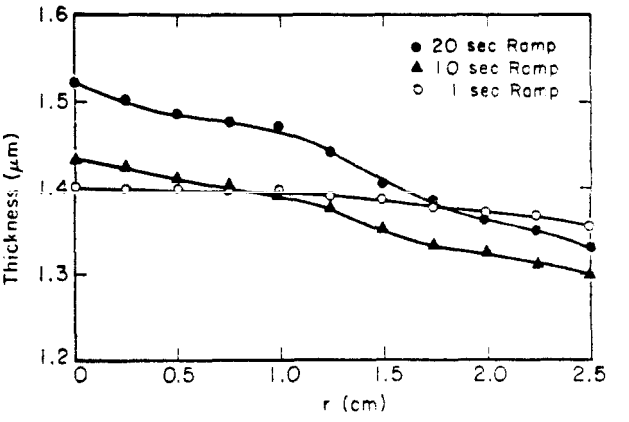

FIG. 10. Experimental film thickness profiles for processes described in Fig. 9 by the model. The expenmental trends are similar to those predicted by the non-Newtonian model.

Having established that the model properly predicts the dependence of final resist thickness on spinner speed, it was of interest to determine to what extent the time allowed for acceleration to the final spin speed influences the final resist thickness and its radial uniformity. Figure 8 illustrates plots of film thickness versus time for 1-, 10-, and 20-s acceleration periods to reach a final speed of 1000rpm. It is evident that the length of the acceleration period strongly influences the initial portion of the thickness-time history but not the final thickness of the film. What is affected by the length of the acceleration period is the radial uniformity of the film. Figure 9 shows that a 1-s acceleration period produces a much more uniform film than acceleration periods of 10 or 20 s. Experimental verification of these effects is shown in Fig. 10. Comparison of Figs. 9 and 10 shows that while the model properly predicts the qualitative effects of lengthening the acceleration period, it overpredicts the degree of radial nonuniformity. The model also fails to predict the presence of waves in the film-thickness profile. Both of these discrepancies are very likely due to the neglect of surface forces at the film-vapor boundary.

SUMMARY

Resist spin coating has been successfully modeled based on a detailed non-Newtonian analysis, allowing local fluid viscosity to vary with concentration and shear rate. Two major thickness reduction mechanisms, convective radial flow and solvent evaporation, have been identified. The former dominates at early stages in the process, while the latter becomes significant towards the end. Predictions based on the model agree quantitatively with experimental observations of the dependence of the film thickness arid profile uniformity on concentration, spinner acceleration characteris-

tics, and final spin speed. Neglect of shear-thinning results in an overprediction of film thickness, underprediction of the effects of spinner speed on film thickness, and an inaccurate prediction of film profile.

ACKNOWLEDGMENTS

This project was supported by the Air Force Office of Scientific Research under Grant AFSOR-90-0078 Mr. Kaveh Pournoor assisted with the early phases of numerical simulation.

[1]A. G Emslie, F. T. Bonner, and L. G. Peck, J. Appl. Phys. **29**, 858 (1958).
[2]A. Acrivos, M. J. Shah, and E. E. Petersen. J. Appl. Phys. **31**, 963 (1960).
[3]L. A. Dorfman, J. Eng. Phys. **12**, 162 (1967).
[4]G. F. Damon, Proceedings of the Kodak Seminar on Microminiatunzation, P-195, **34**, 195 (1969).
[5]N. Fraidenraich, Rev. Mex. Fis. **25**, 69 (1976).
[6]B. D. Washo, IBM J. Res. Dev. **21**, 190 (1977).
[7]P. O'Hagan and W. J. Daughton, in Proceedings of the Kodak Seminar on Microelectronics, G-48, 95 (1977).
[8]D. Meyerhofer, J. Appl. Phys. **49**, 3393 (1978).
[9]W. J. Daughton, P. O'Hagan, and F. L. Givens, Proceedings of the Kodak Seminar on Microelectronics, G-49, 15 (1978).
[10]F. L. Givens and W. J. Daughton, J. Electrochem. Soc. **126**, 269 (1979).
[11]W. J. Daughton and F. L. Givens, J. Electrochem. Soc. **129**, 173 (1982).
[12]H. Fujita, A. Kishimoto, and K. Matsumoto, Trans. Faraday Soc. **56**, 424 (1960).
[13]W. Y. Chiu, G. M. Carratt and D. S. Soong. Macromolecules **16**, 348 (1983).
[14]P. E. Baillagou, M. S. Thesis, University of California. Berkeley. 1983.
[15]P. DeGennes, Scaling Concepts in Polymer Physics (Cornell Univ., Ithaca, 1979).
[16]R. K. Prud'Homme (private communication).
[17]D. Soong and M. Shen, J. Rheol. **25**, 259 (1981).
[18]T. Y. Liu, D. S. Soong, and M. C. Williams. Polym. Eng. Sci. **21**, 675 (1981).
[19]T. Y. Liu, D. S. Soong, and M. C. Williams, J. Rheol. **27**, 7 (1983).
[20]B. J. Wu, D. W. Hess, D. S. Soong, and A. T. Bell, J. Appl. Phys. **54**, 1725 (1983).
[21]CRC Handbook of Chemistry and Physics, 56th ed., edited by R. Weast (CRC, Cleveland, 1975), p. D-231.
[22]B. Maxwell and M. Nguyen, Polym. Eng. Sci. **19**, 1140 (1979).
[23]V. Lütje and G. Meyerhoff, Makromol. Chem. **68**, 68 (1963).
[24]F. Rodriquez, Principles of Polymer Systems McGraw-Hill, New York, 1970), p. 157.